Experimental Validation of Complex Non-Minimum Phase Zeros in Flexure Mechanism Dynamics

Leqing Cui, Dhanushkodi Mariappan, and Shorya Awtar
Precision Systems Design Laboratory, Mechanical Engineering
University of Michigan, Ann Arbor, MI 48109

BACKGROUND AND OBJECTIVE

This research is motivated by the need to achieve large range, high precision, and high speed – all simultaneously – in multi-axis flexure mechanisms. Previous work has shown large range (10mm per axis) and nanometric precision (25nm) in an XY motion system based on a parallel-kinematic flexure mechanism [1]. This mechanism employs a systematic and symmetric layout of eight double parallelogram flexure modules (DPFM), resulting in a high degree of geometric decoupling between the X and Y motion axes. But experimental frequency response measurements of the X direction transfer function relevant for motion control exhibit complex non-minimum phase zeros (CNMP) at certain Y direction operating points. These CNMP zeros are highly detrimental to the closed-loop dynamic performance of the motion system including bandwidth and stability robustness [2].

To understand the conditions under which such CNMP zeros arise and determine if physical design decisions can eliminate these zeros, a representative XY flexure mechanism (Fig. 1) has been recently investigated [3]. This design is relatively simpler but has all the essential attributes of the original XY flexure mechanism [1], including multi-axis motion capability (X and Y) and at least two DPFMs in a nominally symmetric configuration that lead to closely spaced modes. The non-collocated transfer function from the force P to displacement X_1 was examined, as a function of cross-axis operating point Y_{1o}, via lumped-parameter non-linear dynamic modeling. A static Y direction force F_0 was assumed on the motion stage (stage 1) to establish this non-zero Y direction operating point (Y_{1o}). It was shown that the geometric non-linearity associated with arc-length conservation in flexure beams along with the kinematic under-constraint in the DPFM result in a coupling between the Y motion of the secondary stages (2 and 3 in Fig.1) and the X motion of the motion stage for non-zero operating points (Y_{1o}). Furthermore, the two closely spaced modal frequencies associated with the Y motions of the secondary stages of the two DPFM were varied by introducing an intentional parametric asymmetry (mass difference between stages 2 and 3, given by $\Delta m_{23} = m_2/m_3 - 1$) to simulate practical manufacturing tolerances.

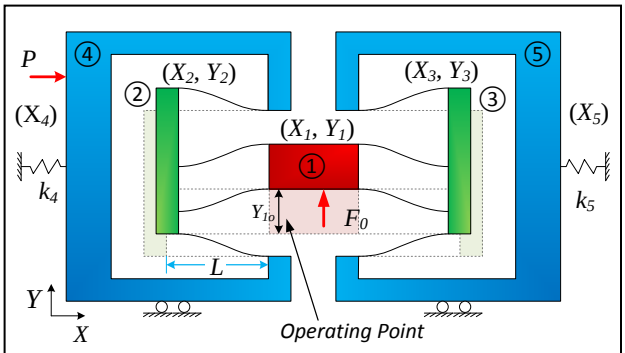

Fig.1. Simple Representative 4 Degree-of-Freedom (SR4DoF) XY Flexure Mechanism

This model showed that these closely spaced modes interact as the above mentioned coupling varies with the operating point and as the parametric asymmetry varies, giving rise to CNMP zeros under certain conditions. This is illustrated in Fig.2, which maps the existence of CNMP zeros against a range of operating points (Y_{1o} normalized with respect to beam length L) and parametric asymmetry (Δm_{23}). Black regions on this map indicate the presence of CNMP zeros. This map indicates that one can intentionally choose the physical design parameters (e.g. $\Delta m_{23} < 0$) to eliminate the CNMP zeros, enabling better dynamic performance (i.e. higher speed, bandwidth, and stability robustness). This paper presents an experimental validation and confirmation of these modeling predictions.

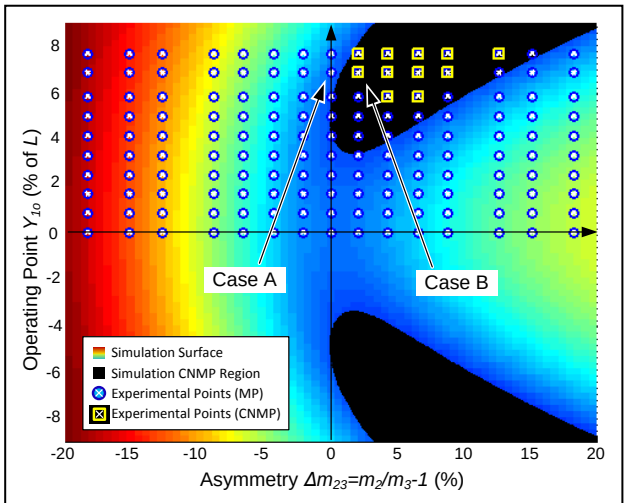

Fig.2. Complex Non-Minimum Phase Zero Map

EXPERIMENTAL SETUP DESIGN

The goal of the experimental setup design is to minimize factors such as noise, disturbance, undesired modes, parasitic dynamics, etc. so that one can focus on and validate the specific CNMP phenomenon predicted by the above referenced model. Key hardware design challenges addressed in this effort are: (i) The theoretical roller and spring functionalities in Fig.1 are achieved via simple flexure bearings to eliminate friction and backlash; (ii) The geometry and dimensions of the overall flexure mechanism are iteratively selected to isolate the modes associated with the secondary stages 2 and 3 from other modes. Isolating these two "modes of interest" helps provide a "clean" observation of their interaction and allows an investigation into the genesis of CNMP zeros; (iii) The constant Y direction force (F_0) is implemented via a long steel cable loaded by a free-hanging weight with a virtual pulley [4], which effectively prevents parasitic dynamics and offers frictionless loading.

Overall Flexure Mechanism Geometry

For ease of discussion, we use the term *main flexure* to refer to stage 1 through stage 5 in Fig.1, including the two DPFMs. Fig.3 illustrates the design evolution of the overall flexure mechanism, comprising the main flexure that is designed for conducting the relevant experiments. Starting with Fig.3a, the initial configuration of the SR4DoF flexure mechanism is shown using two springs and rollers that connect the main flexure to the ground. In order to eliminate friction and backlash, the springs and rollers are replaced by four simple flexure beams in Fig.3b. However, such design has limited travel range in the X direction due to geometric over-constraint of the flexure beams. To relieve this over-constraint, the simple beams are replaced by folded beams in Fig.3c. However, the folded beams offer low translational stiffness along the Y-axis and low rotational stiffness about the Z-axis. This leads to additional undesired low frequency modes. In Fig.3d, these folded beams are replaced with DPFMs, since the latter offer better stiffness characteristics without sacrificing travel range. In order to avoid rotational modes about the X axis, as shown in Fig.3d, or rotational modes rotation about the U-axis, as shown in Fig.3e, four *minor* DPFMs are used symmetrically in the design of Fig.3f. The term *minor* is used in order to distinguish these four DPFMs from the two DPFMs in the main flexure of Fig.1. The tradeoff here is a slightly higher stiffness (k_4 and k_5) in the X direction of the overall flexure mechanism, which leads to a higher frequency of the X direction rigid body mode of the overall flexure mechanism. This has to be taken into consideration as we aim to isolate the two modes of interest associated with the secondary stages of the main DPFMs from rest of the modes, as described next.

Overall Flexure Mechanism Dimensions

Once the overall flexure mechanism design was conceptually established, the detailed dimensions were optimally selected as follows.

(1) We started with choosing the dimensions of the main flexure beams (Fig.3g) to be the same as that in the original XY flexure mechanism that motivated this investigation [1, 3]. Accordingly, the length of the main beam was set at L_1=47.5mm and thickness was set at T_1=0.625mm.

(2) The mass of each stage in the main flexure (Fig.1) was selected so as to isolate the two modes of interest (3rd and 4th modes in Fig.4) from the first two modes (1st and 2nd modes in Fig.4). This was

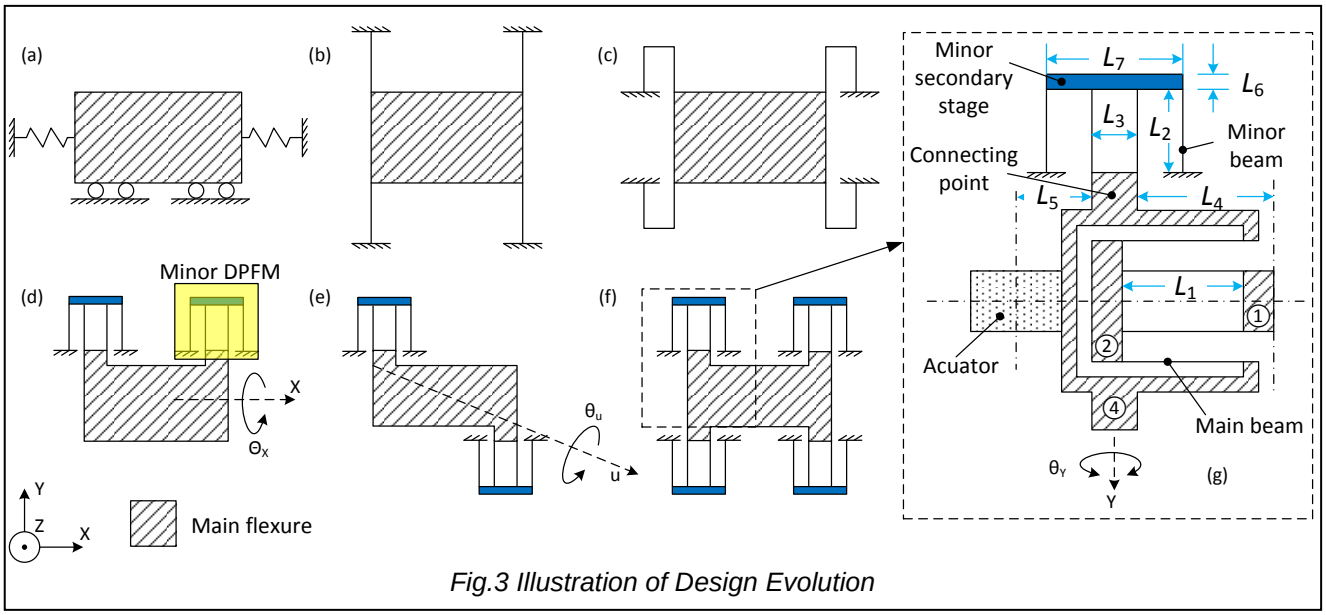

Fig.3 Illustration of Design Evolution

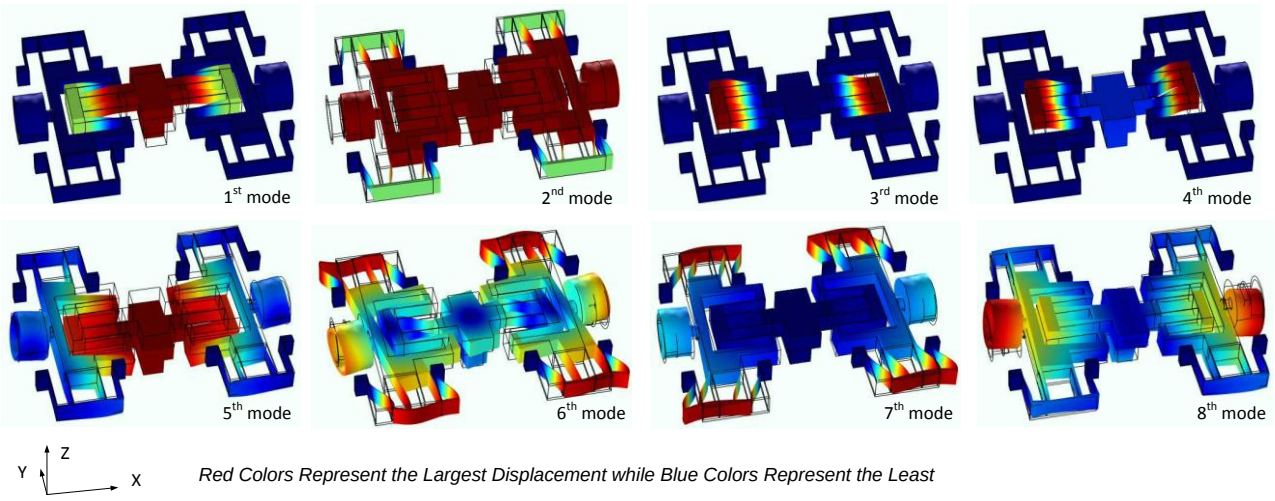

Fig.4 Mode Shapes of the Final Design

TABLE.1 Key Dimensions, Corresponding Natural Frequencies and Mode Orders

Dimensions (mm)						Mode order and natural frequencies (Hz)							
L_2	T_2	L_3	L_4	L_6	L_7	1st	2nd	3rd	4th	5th	6th	7th	8th
47.5	1	40	85	3	80	21	31	80	84	213	231	271	272

accomplished by setting m_1=0.4kg, m_2=m_3=0.06kg, and m_4=m_5=0.78kg. The 3rd and 4th modes are the closely spaced modes of interest that we intend to investigate in this study.

(3) Furthermore, it was desirable to set the natural frequencies of the modes associated with the vibration of the secondary stages of the four minor DPFMs to be much higher than the two modes of interest. To increase these resonance frequencies, one can either increase the transverse stiffness of the minor beams or reduce the mass of the minor secondary stages. The former approach increases the frequency of primary X direction rigid body mode (2nd mode in Fig.4) bringing it closer to the modes of interest, while the latter results in a smaller L_6, which increases the compliance of the minor secondary stages and introduces additional undesired modes at lower frequencies. This tradeoff was addressed by iteratively selecting dimensions and checking the mode shapes and frequencies. In the final design, we chose L_2=47.5mm, T_2=1mm (thickness of minor beam), L_6=3mm, and L_7=80mm.

(4) The choice of dimensional values for L_3, L_4 and L_5 (see Fig.3g) is based on the consideration that the rotational modes about the Y and Z axes should be kept much higher than the modes of interest. Therefore, the span L_3 of the inner minor beams has to be large enough (within layout size constraints) to ensure that rotational stiffness of the minor DPFM about the Y and Z axes is high. Furthermore, dimensions L_4 and L_5 have to be chosen so that moment of inertia contributed by stages 1, 2, 3, 4, and 5 about the Y and Z axes is minimized. Accordingly, we chose L_3=40mm, L_4=85mm and L_5=30mm in the final design to meet the requirements outlined here.

Summary of Mode Orders and Frequencies

Table.1 summarizes the dimensions selected for the final design, and the resulting mode orders and frequencies of the overall flexure mechanism (Fig.3f).

The 1st mode is the in-phase Y direction vibration of stages 1, 2 and 3. Therefore, this mode makes a negligible contribution to the frequency response measurement at stage 1 in the X direction. The 2nd mode is the primary X direction 'rigid-body' of the overall flexure mechanism. This mode shows up as the second mode due to the increased X direction stiffness of the minor beams, based on criterion (3) discussed above.

The 3rd and 4th modes are the modes associated with the vibration of two main secondary stages, which are the modes of interest in this paper.

The 5th mode is an out-of-plane mode in the Z direction while the 6th mode is an in-plane rotational mode about the Z direction. Next, there are four modes associated with the X direction vibration of the four minor secondary stages. These are the 7th (271 Hz), 9th (283 Hz), 12th (286 Hz), and 14th (307 Hz) modes. There are several other modes in between these four modes given the choice of dimensions. For example, the 8th mode comprises out-of-plane rotation about the Y direction.

In summary, in the final design, there is at least a two-times frequency separation before and after the closely spaced modes (3rd and 4th) of interest,

offering a satisfactory isolation from the other modes. Therefore, the dimensions in Table 1 were employed in the fabrication of the final experimental setup hardware.

Constant Force Loading Mechanism

For the SR4DoF XY mechanism shown in Fig.1, the operating point is set by applying a static Y direction force F_0. One of the challenges in applying such a constant force on the motion stage is that the latter's position varies along the X and Y axes. During the frequency response measurement, the motion stage vibrates in the X direction with a small amplitude in response to an excitation in the X direction. Also, due to cross-axis coupling, there can be an even smaller but finite Y direction vibration at the motion state in response to an X direction excitation. The Y direction actuation system has to accommodate these X and Y direction displacements during a frequency response measurement. Furthermore, since this measurement has to be repeated at various Y direction operating points (Y_{1o}=±5mm), the Y direction actuation system has to be capable of providing the necessary force (F_o) over this range and hold it constant at a given operating point.

Instead of employing an electromagnetic actuator to apply a constant force, we chose a relatively simpler actuation method utilizing steel braided cables and free weights. However, this method requires the use of a pulley to change the direction of force provided by the weights. Since a traditional pulley introduces displacement uncertainty in the loading direction due to rolling and/or sliding friction, we used a frictionless virtual pulley instead [4].

Fig.5 shows the schematic of the virtual pulley arrangement comprising three cable segments: a long horizontal segment, a vertical segment, and a diagonal segment. All three segments are connected at a common point. The other end of the horizontal segment is attached the motion stage; the other end of the vertical segment is connected to a hanging weight; and the other end of the diagonal segment is connected to a rigid extension of the ground reference (e.g. optics table). This cable arrangement is called a virtual pulley because

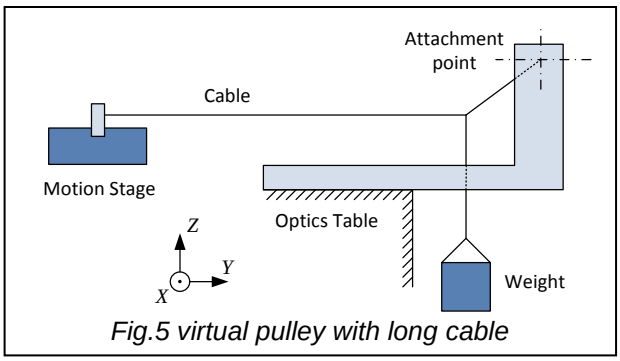

Fig.5 virtual pulley with long cable

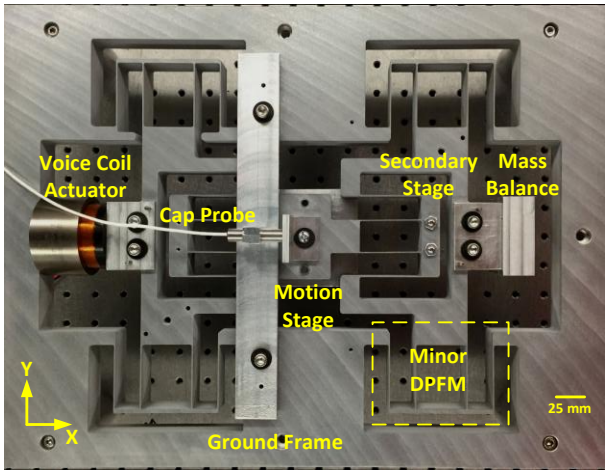

Fig.6. Experimental Setup Hardware

it converts the vertical force of the weight in the Z direction to a horizontal force F_o on the motion stage in the Y direction. The two are simply related by the trigonometry of the cable arrangement. In this manner, a constant Y direction force F_o is achieved by a known hanging weight, without the need for any active force control. The horizontal section of the cable was selected to be long enough so that it can absorb any X direction displacement of the motion stage without appreciably impacting the F_o force. Any Y direction vibration of the motion stage is also easily accommodated by the virtual pulley. The Y direction operating point is varied simply by changing the weight, and keeping track of any change in the cable arrangement trigonometry. Thus, the virtual pulley provides a frictionless pulley functionality because it eliminates any rolling or sliding interfaces and any associated uncertainties.

RESULTS AND DISCUSSION

The experimental setup hardware was fabricated and assembled for testing, as shown in Fig.6. The flexure mechanism along with the reference ground frame was made monolithically from a 25.4mm thick AL6061-T651 plate using wire-electric discharge machining (EDM), which allows dimensional tolerance of ± 0.005 mm. With the given dimensions and desired range of motion, the factor of safety against yielding was greater than 2.

The displacement of the motion stage in the X-axis was measured by a capacitance probe (Lion Precision, Range: 2 mm, Peak-peak resolution 400 nm, RMS resolution: 40 nm) mounted on a fixture attached to the ground frame. Thus the X direction displacement measurement of the motion stage with respect to the ground is not affected by the large Y direction displacement (up to ± 5 mm) of the motion stage.

A voice coil actuator (BEI Kimco Magnetics, LA24-

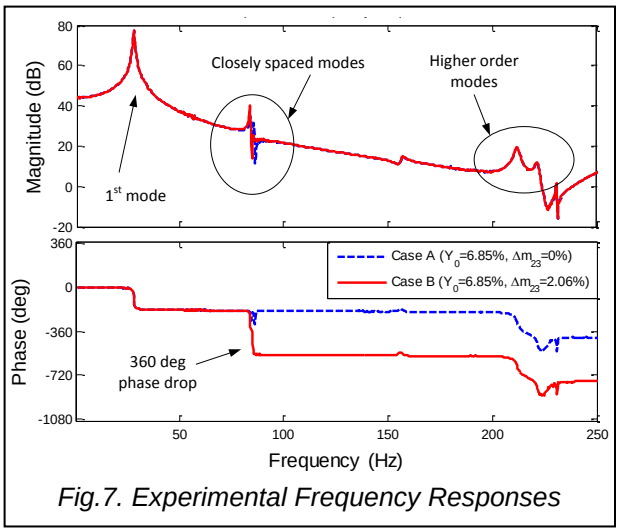

Fig.7. Experimental Frequency Responses

20-000A, Force constant: 11.12 N/A, Stroke: ± 8.26 mm) was selected for the X direction actuation. A custom-built current amplifier based on the Power OpAmp MP111 was used to drive current in the voice coil actuator at a bandwidth of 1 kHz [1]. The system was controlled using a DSpace 1103 real-time control system with a loop-rate of 1 kHz. Frequency domain transfer function measurement was performed using a chirp signal as the input. The input and output time-domain signals were then processed using the system identification toolbox of MATLAB to obtain the frequency responses.

Fig.7 shows the experimental frequency response from the actuator force P to the X direction displacement (X_1) of the motion stage (see Fig.1), for two sets of operating points and mass asymmetries. The mass asymmetries are achieved by adding additional mass on the main secondary stages. Key observations are: (i) the first four experimentally measured modes match well with the above-described model; (ii) the closely spaced modes of interest are well-separated from other modes, as expected from the overall flexure mechanism design; (iii) CNMP zeros are witnessed as predicted by the prior modeling effort. For example, Case A, which corresponds to Y_{1o} = 6.85% of beam length and symmetric masses (i.e. Δm_{23} = 0) shows no CNMP zeros, while Case B, which corresponds to Y_{1o} = 6.85% and Δm_{23} = 2.06%, exhibits CNMP zeros at frequencies close to the two modes associated with the secondary stages (2 and 3) of the main DPFMs.

In Fig.2, the multiple experimental findings are overlaid on the model predictions. Note that only half of the area is tested due to the symmetric properties of the flexure with respect to positive/negative operating points. The squares indicate the conditions when CNMP zeros are present in the frequency response, while the circles indicate conditions when CNMP zeros are absent, as measured experimentally. Fig.2 shows that the experimental results match well with the model prediction: (i) For negative asymmetry (Δm_{23}<0), the entire operating range is free of CNMP zeros; (ii) For Δm_{23}>0, experimental findings largely agree with model prediction of the CNMP zero region and confirm that CNMP zeros appear only when the operating point is larger than a certain value; (iii) When nominally symmetric (Δm_{23}≈0), the frequency response is very sensitive to mass parameter variation in terms of the existence of CNMP zeros at large operating points.

The minor mismatch between the experimental and predicted CNMP region in Fig.2 maybe attributed to: (i) The parameter grid resolution used in testing, and (ii) Imperfection in the flexure setup due to manufacturing and assembly tolerances.

CONCLUSION

This work has experimentally validated the previous model-based prediction [3] of the existence of CNMP zeros in the flexure mechanism of Fig.1 for certain specific combinations of parametric asymmetry and operating point. Significantly, this work shows that via an intentionally asymmetric choice of secondary stage masses, one can completely eliminate the CNMP zeros, thereby enabling better closed-loop dynamic performance. Furthermore, since the flexure beams are still symmetric, the quasi-static performance (which is independent of masses) in terms of cross-axis decoupling and error motions at the motion stage can still be preserved.

REFERENCES

[1] S. Awtar and G. Parmar, "Design of a Large Range XY Nanopositioning System," *Journal of Mechanisms and Robotics,* vol. 5, pp. 021008-021008, 2013.

[2] J. S. Freudenberg and D. P. Looze, "Right Half Plane Poles and Zeros and Design Trade-offs in Feedback Systems," *IEEE Transactions on Automatic Control,* vol. 30, pp. 555-565, 1985.

[3] L. Cui, C. Okwudire, and S. Awtar, "Complex Non-Minimum Phase Zeros in the Dynamics of Double Parallelogram Flexure Module Based Flexure Mechanisms," in *ASME 2016 Dynamic Systems and Control Conference*, Minneapolis, Minnesota, Paper # DSCC2016-9658.

[4] S. Awtar, "Synthesis and Analysis of Parallel Kinematic XY Flexure Mechanisms," Massachusetts Institute of Technology, 2004.